JACS
JOURNAL OF THE AMERICAN CHEMICAL SOCIETY

ARTICLE

pubs.acs.org/JACS

Probing Coherence in Synthetic Cyclic Light-Harvesting Pigments

Jessica E. Donehue,[†] Oleg P. Varnavski,[†] Robert Cemborski,[†] Masahiko Iyoda,[‡] and Theodore Goodson, III*[,†]

[†]Department of Chemistry, University of Michigan, Ann Arbor, Michigan 48109, United States

[‡]Department of Chemistry, Graduate School of Science and Engineering, Tokyo Metropolitan University, Hachioji, Tokyo 192-0397, Japan

Supporting Information

ABSTRACT: A series of π-extended cyclic thiophene oligomers of 12, 18, 24, and 30 repeat units have been studied using methods of ultrafast time-resolved absorption, fluorescence upconversion, and three-pulse photon echo. These measurements were conducted in order to examine the structure−function relationships that may affect the coherence between chromophores within the organic macrocycles. Our results indicate that an initial delocalized state can be seen upon excitation of the cyclic thiophenes. Anisotropy measurements show that this delocalized state decays on an ultrafast time scale and is followed by the presence of incoherent hopping. From the use of a phenomenological model, we conclude that our ultrafast anisotropy decay measurements suggest that the system does not reside in the Förster regime and coherence within the system must be considered. Three-pulse photon echo peak shift experiments reveal a clear dependence of initial peak shift with ring size, indicating a weaker coupling to the bath (and stronger intramolecular interactions) as the ring size is increased. Our results suggest that the initial delocalized state increases with ring size to distances (and number of chromophores) comparable to the natural light-harvesting system.

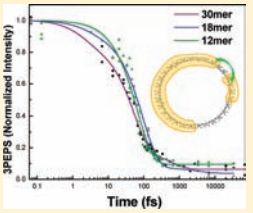

INTRODUCTION

Recent discoveries have indicated that quantum coherence effects may play an important role in achieving remarkably high energy conversion efficiency in natural photosynthetic organisms.[1−6] By effectively linking the chromophores together, quantum coherence allows the molecules to exploit the energy of the sun with nearly 100% efficiency.[2,4,6,7] What remains unclear, however, is an understanding of how specific structural or environmental parameters can contribute to quantum coherence and how these parameters could be synthetically manipulated to increase efficiencies in future optical and electronic devices.

Many oligo- and polythiophene compounds have attracted recent interest for use in optical and electronic devices due to their reported fluorescence and conducting properties.[8−11] The properties of shorter oligomers are known to be greatly influenced by "end-effects".[10,12,13] Dendritic structures have also been studied to determine their potential for use in artificial light-harvesting systems.[14−17] These structures have the advantage of controlled synthesis that results in regular and well-defined architectures, and their photophysical processes are strongly affected by their geometrical confinement.[17−20] However, issues related to end effects and very high flexibility are known to limit the possibilities of these structures.[21] Cyclic molecular aggregates, however, are well-known to play a crucial role in very efficient natural photosynthetic systems.[22,23] Previous studies have shown that long conjugation associated with relatively rigid and ordered cyclic morphology in synthetic structures leads to strongly enhanced nonlinear optical responses.[24−27] Recently developed thiophene-based macrocycles offer new materials that combine potentially endless π-conjugation paths with structurally well-defined oligomers.[28−31] The outstanding electrical properties of oligothiophene systems have already shown success in organic photovoltaic cells.[9,32] By combining these materials with a cyclic topology shown to be efficient in light-harvesting antenna,[33] we are able to gain a novel perspective in the development of efficient light conversion devices that utilize quantum coherence.

In this contribution, we provide a systematic study of π-extended cyclic thiophene oligomers, which include 12, 18, 24, and 30 repeat units (Figure 1). These are π-conjugated systems with nanometer-sized cavities.[24,28,29] The ring diameters vary from ∼21 to ∼60 Å.[24,28,29] These materials experience no "end-effects" and are expected to be more rigid as compared to linear oligomers. To better understand the role of synthetic parameters, like ring size, in electronic coherences, we have preformed a detailed investigation of the structure of optical excitation in the artificial ring systems using ultrafast polarization- and time-resolved absorption, fluorescence, and three-pulse photon echo. The electronic delocalization length is an important measure of the balance between the electronic intrachain coupling and the bath coupling (two fundamental interaction mechanisms that determine the efficiency of energy transfer in a light-harvesting system)[1−7,22,23,34−36] in a given oligomeric system[36,37] and therefore is a main focus in this work. Higher delocalization lengths indicate that more sites are contributing to quantum coherence effects in the energy transfer process. States delocalized over a larger number of repeat units can possess larger transition moments, which facilitate greater absorption in a light-harvesting system and high energy transfer rates (hopping) between spectroscopic units. This can lead to a larger excitation

Received: September 16, 2010
Published: March 08, 2011

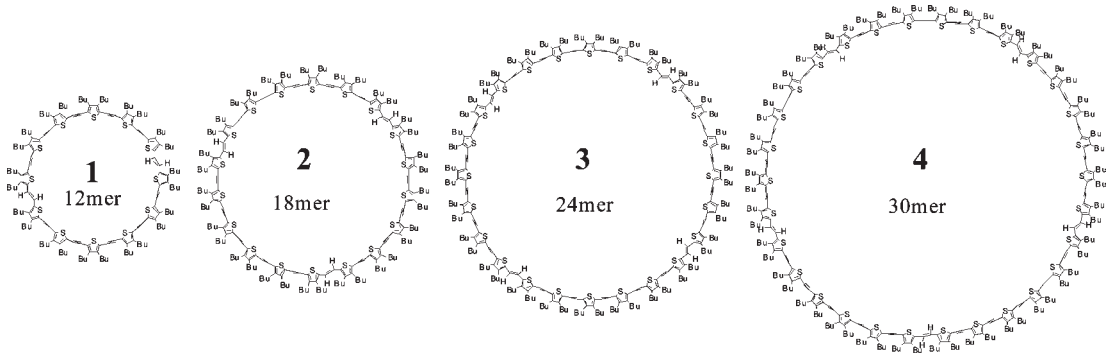

Figure 1. Structures of giant thiophene macrocycles.

migration distance, a parameter critical for efficient photovoltaics. With synthetic control of the ring size in the artificial structures, we will gain insight into the electronic delocalization length, as well as the role of planarity and the optimal number of building blocks in a ring, to maximize the optical response at lower cost. A more detailed understanding of these parameters is central to gaining deeper insight into quantum coherence-assisted energy transfer and how it can be incorporated into the design of artificial light-harvesting materials to direct energy flow with high efficiency.

Importantly, we have found the initial peak shift to increase as the size of the cyclic oligomer increases. As the initial peak shift reflects the inverse effective electronic transition−bath interaction,[38−40] the peak shift rise indicates a decrease of the effective coupling of the electronic transition to the bath for larger rings. We assign this trend to the larger size of the electronic excitation coherent domain in larger rings. The delocalized excitation results in the eigenstate averaging over the fluctuations in local inhomogeneities of the sites,[36,38−43] leading to the increased initial peak shift. Combined with all ultrafast methods used in this study, these results indicate an initial delocalized state upon excitation of the cyclic oligomers.

EXPERIMENTAL SECTION

Synthesis and Structural Characterization. In this work, we have investigated π-extended cyclic thiophene oligomers of 12, 18, 24, and 30 repeat units (Figure 1, **1**−**4**). These materials were first synthesized by Iyoda and co-workers.[28,29] The synthesis of **1**−**4** was carried out by a McMurry coupling reaction with low-valent titanium.[24] All macrocycles presented possess key stability and oxidative characteristics[24] necessary for use in molecular electronics. They have fairly low oxidation potentials ($E^1_{1/2}$ = 0.31−0.33 V; $E^2_{1/2}$ = 0.50−0.52 V vs Fc/Fc^+).[24] All macrocycles are stable in crystalline form in air at room temperature. The X-ray structure has been measured for a single crystal of **1** obtained from chloroform−hexane solution.[24]

Steady-State Measurements. Unless stated otherwise, all the experiments were performed in THF at ambient temperature. The absorption spectra of the molecules were recorded using an Agilent (Model # 8341) spectrophotometer. The emission spectra were acquired using a Shimadzu RF-1501 instrument. The quantum yields of the molecules were measured using a known procedure.[44] Coumarin 307 was used as the standard. The absorbance was limited to less than or equal to 0.03.

Transient Absorption Measurements. Time-resolved degenerate transient absorption studies have been carried out utilizing a cavity dumped Ti:sapphire laser system, which is spectrally centered at 830 nm with a repetition rate of 38 kHz and a pulse width of ∼20 fs.[45,46] The fundamental beam was passed through a nonlinear BBO crystal generating the second harmonic, which was used as the excitation beam. This system possessed good noise characteristics, allowing the sensitivity for relative transient absorption in the 10^{-7} range at very low pump pulse energy, <0.5 nJ/pulse. A probe beam of the same wavelength was passed through an optical delay line and a lens before being overlapped with the pump beam in the sample cell and detected by a photodiode. The modulated probe signal was measured with the use of a lock-in amplifier synchronized to an optical chopper in the pump beam path and was recorded as a function of delay line on a PC. Fitting the Gaussian peak of the instrument response function (IRF) gave a σ value of ∼33 fs (fwhm ∼82 fs).[45,47] Polarization of the probe beam was controlled with a Berek compensator. For polarization measurements, the setup was calibrated with the linear molecule β-carotene.

Femtosecond Time-Resolved Fluorescence Upconversion. Time-resolved polarized fluorescence of the thiophene macrocycles was studied using the femtosecond upconversion spectroscopy technique.[48] The upconversion system used in our experiments has been previously described.[26,45] Specifically, our upconversion system used frequency-doubled light from a mode-locked Ti:sapphire laser that produced pulses of 100 fs at a wavelength of 385−430 nm. Polarization of the excitation beam for the anisotropy measurements was controlled using a Berek compensator, and the rotating sample cell was 1 mm thick. Horizontally polarized fluorescence emitted from the sample was upconverted in a nonlinear crystal of β-barium borate using a pump beam at about 800 nm, which was first passed through a variable delay line. The instrument response function (IRF) was measured using Raman scattering from water. Fitting the Gaussian peak from the Raman scattering yields a σ value of a Gaussian IRF of ∼106 fs, giving a full width at half-maximum of ∼243 fs. Spectral resolution was achieved by using a monochromator and photomultiplier tube. The excitation average power varied near 1 mW, corresponding to a pulse energy around a few tens of picojoules per pulse.

Three-Pulse Photon Echo Measurements. Three-pulse photon echo experiments were carried out using a cavity-dumped Kerr lens mode-locked Ti:sapphire laser pumped by a frequency-doubled YVO laser (Millennia, Spectra Physics).[45] The cavity-dumped laser pulse had a duration of ∼20 fs. The pulse spectrum was centered at ∼830 nm. The cavity dumped beam was focused onto a 0.5 mm BBO crystal to convert the fundamental beam into the second harmonic at ∼415 nm. Unless mentioned otherwise, the pulse repetition rate after cavity dumper was fixed at 38 kHz. In our setup, three beams of equal intensities (∼0.5 nJ per pulse in one beam at the sample) were generated with the aid of thin beam splitters (1 mm-thick quartz substrate, CDP). One pulse (k_1) traveled a fixed delay, whereas the other two pulses (k_2 and k_3) traveled variable delays formed with retro-reflectors mounted on dc-motor driven delay stages (Newport ILS100CCHA) controlled via a Newport ESP7000 motion controller. The three beams were aligned after the delay stages to form an equilateral triangle beam geometry (8 mm sides) and were focused into the 440 μm quartz sample cell using

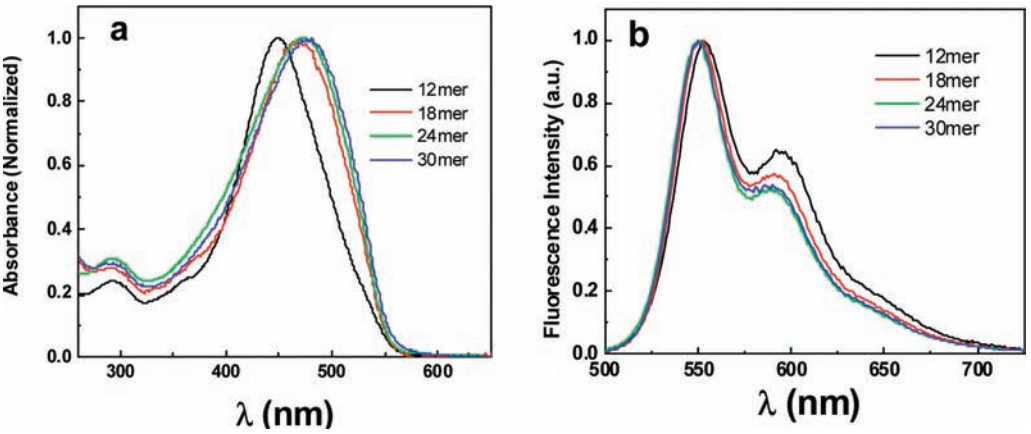

Figure 2. Normalized absorption (a) and fluorescence (b) spectra of the macrocycles 12mer−30mer.

a thin singlet lens (f = 18 cm). The two third-order nonlinear signals in the $k_1 - k_2 + k_3$ and $-k_1 + k_2 + k_3$ phase-matching directions were spatially filtered using irises and measured simultaneously onto two photomultipliers (Hamamatsu Photo Sensor Modules H6780). The electrical signals were measured by two lock-in amplifiers (Stanford Research, SR830) that were referenced to a chopper (SR540) inserted in the k_1-beam. Reproducibility of the signal was confirmed by repeated measurements, with special attention paid to the residual peak shift value at long population periods T. The uncertainties of the peak shift value were estimated to be approximately ±0.5 fs over the entire population period up to 100 ps. The absorption spectra of the samples were checked before and after data collection and lack of any observable changes, suggesting that little or no sample photodegradation or undesired chemical reactions occurred during the measurement. For our three-pulse photon echo peak shift experiment, we simultaneously recorded two echo signals at the phase-matching conditions $k_1 - k_2 + k_3$ and $-k_1 + k_2 + k_3$. The time period τ between pulses 1 and 2 was scanned from negative τ to positive τ for a fixed population period T. The peak shift was defined as half the distance between the maximum intensity peaks of the two echo signals. The peak shift was recorded as a function of population period to give a peak shift decay. This measure is useful in that it closely follows the frequency fluctuation correlation function of the transition.[38−40]

■ RESULTS AND DISCUSSION

Linear Spectroscopy. The normalized steady-state absorption and emission spectra of the structures are shown in Figure 2. Steady-state measurements were performed in dilute THF solutions (ca. 10^{-6} M). The position of the main peak in absorption shows a bathochromic shift with increasing size of the macrocycle. While the fluorescence spectra of the 12mer appears to have some small red shift with respect to the other ring systems, the fluorescence spectra of the 18mer, 24mer, and 30mer do not demonstrate any systematic shift. This small red shift in the 12mer fluorescence, as well as a blue shift in its absorption spectrum as compared to other rings, can be associated with the specific "ring flip" of the thiophenes adjacent to flexible double bonds. This is known to relieve strain in the 12mer.[24] The strain is less for larger spatial arrangements,[28,49] which leads to more regular structures.[24,28] This blue shift in the 12mer absorption could also be due to symmetry reasons and relatively large distances between excitonic states.[66] Clear vibronic structure can be observed in the fluorescence spectra (∼1300 cm^{-1}) and is similar to that reported for variously sized linear oligo(thienylene-ethylene)s.[50,51] However, no vibronic structure is seen in the absorption spectra. This absence of mirror symmetry between absorption and emission spectra may indicate different absorption (Franck−Condon) and fluorescence (relaxed) configurations.[52,53] The similarity in fluorescence spectra for the rings of different sizes (18mer−30mer), as well as nearly the same fluorescence quantum yield (∼10%) for all sizes, can be due to the localized character of the fluorescent (relaxed) state in these systems.

Interestingly, the fluorescence peak for the macrocycles (560 nm) is shifted to the red with respect to that for linear oligo(thienylene-ethynylene)s (512[50] and 513 nm[28]). This red shift may indicate longer conjugation length in the rings as compared to the linear building block.[50] It is also worth noting that the Stokes shifts for the 18mer (3285 cm^{-1}), 24mer (3032 cm^{-1}), and 30mer (2944 cm^{-1}) are substantially smaller than those for the linear oligo(thienylene-ethynylene)s [3565 cm^{-1} for 5αTE,[50] 3617 cm^{-1} for 9αTE39,[50] and 3602 cm^{-1} for oligo(2,5-thienylene-ethynylene)[28]]. The corresponding smaller reorganization energies for the macrocycles, as compared to linear counterparts, could be an indication of less structural change for the macrocycles due to the absence of open ends and more rigid structure.

Ultrafast Transient Absorption. We have investigated the polarized degenerate transient absorption dynamics at 415 nm as a function of macrocycle size. In Figure 3, multiexponential anisotropy decays can be seen for both the 12mer and the 30mer. We have preformed a best fit of the data with multiexponential decays after assuming the convolution of the IRF with the parallel and perpendicular absorption intensity profiles (see the Supporting Information). The 12mer macrocycle was best modeled by a biexponential decay with an ultrafast component and a long-lived residual component. The 18mer, 24mer, and 30mer macrocycles were best modeled by three exponential decays, which included an ultrafast component, an additional picosecond component not seen in the 12mer decay, and a long-lived residual value.

The ultrafast decay component in each macrocycle was found to be in the range between 40 and 50 fs. This ultrafast depolarization can be associated with strong interchromophore interaction and formation of a delocalized state (spectroscopic unit) over a substantial portion of the macrocycle.[17,25,34,45,46] The second decay component found in the larger (18mer, 24mer, and 30mer) macrocycles was near ∼1 ps. The appearance

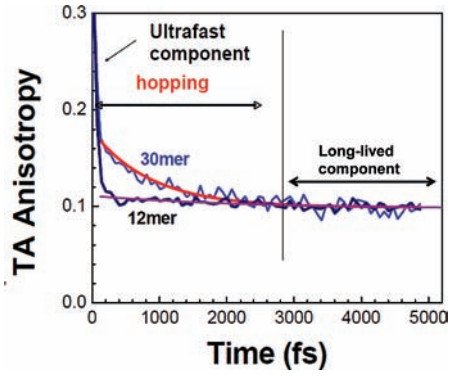

Figure 3. Degenerate time-resolved transient absorption anisotropy for thiophene 12mer and 30mer macrocycles.

of an additional picosecond component in the anisotropy decay profile for the larger rings indicates a hopping between spectroscopic units that is smaller than the full size of the ring.[23,45] In the case of the 12mer, the size of the spectroscopic unit is comparable to the size of the ring, thus making hopping not possible. This observation, as well as the ultrafast decay of the 12mer anisotropy to a residual value of ~0.1, supports the idea of a strong coupling regime with the excitation delocalized over the entire ring in the absorption configuration.[25,26]

The longest decay component was >100 ps and contributed a near flat residual value on a short time scale (Figure 3). Considering the size of the macrocycles and the viscosity of THF (~0.46 cP at 25 °C), this component can be associated with the rotational diffusion of the system. It is also important to note that the residual anisotropy before rotational diffusion occurs is 0.1 for both the 12mer and 30mer macrocycles (Figure 3). This is an indication of a planar arrangement of the transition moments in both molecules.[54] Though the 12mer displays a slightly bent chairlike structure in a single crystal,[24] this can simply be the result of the packing force in the crystalline sample, which could not be present in solution. While in solution, however, the structure remains planar in terms of its transition dipoles' arrangement.

In order to analyze the nature of optical excitations and the electronic coupling within the macrocycles, we utilized a simple phenomenological model developed by Leegwater for multichromophoric ring systems.[34] In this model, the discussion of the coherence of excitations is led by using an expression in which the limiting cases of Förster transfer (weak interaction) and completely delocalized excitonic states (strong interaction) are continuously connected to one another. The analysis uses the high-temperature approximation for the extremely small phonon correlation time.[34] This model has been developed for the optical excitations in aggregates of chromophores where electron−hole pairs after excitation are localized on individual chromophores (Frenkel excitons). The thiophene macrocyclic systems investigated in this work have a substantial degree of conjugation that suggests strong electronic correlations over the oligomer. Though Leegwater's model is a simplified model for the thiophene macrocycles, it uses the exciton approach, which is known to describe some basic features of the electronic structure of conjugated oligomers and polymers (such as energy dependence) quite well.[55,56] For this reason, using Leegwater's model allows for a crude initial estimation of the intracycle coupling strength (transfer integral) and the excitation energy migration regime.[17] An interesting conclusion of this simple approach is that it is possible to relate the depolarization time to the ratio J/Γ

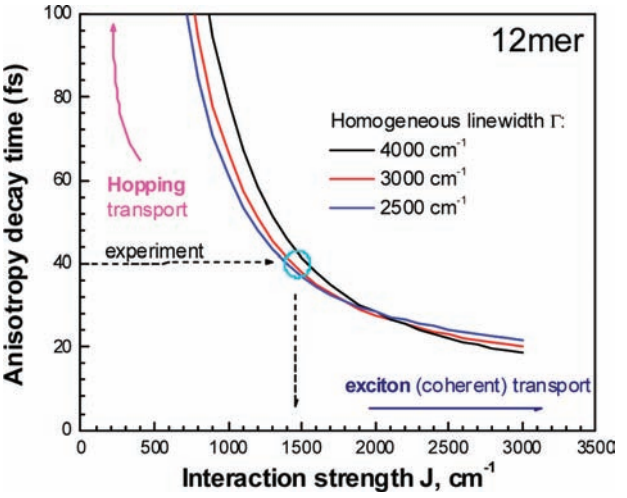

Figure 4. Theoretical dependence[47] of the anisotropy decay time τ_r on the interchromophore interaction J for a macrocyclic 12-chromophore molecular system. The arrow shows the depolarization time obtained from experiment for the 12mer.

of the interaction strength (J) and the homogeneous line width (Γ).[34] For the case of N-fold symmetry (planar) they are related by[34]

$$t_{dep} = \frac{1}{\Gamma(1-A)} \qquad (1)$$

where

$$A = \frac{1}{N}\sum_{k=1}^{N} \frac{\Gamma^2}{\Gamma^2 + 16J^2 \sin^2(2\pi/N) \sin^2(2\pi k/N)}$$

Here N is the number of chromophores contributing to the energy migration process. We have calculated the profile of eq 1 against realistic values of the homogeneous line width for the case of the 12mer (N = 12) macrocycle. Shown in Figure 4 are the calculated curves for eq 1 vs the interaction strength J. As we mention above, a depolarization time of approximately 40 fs was found. To estimate the interaction strength J and energy transfer regime, we need to know the homogeneous line width Γ. Using the full line width instead of the homogeneous line width would be an overestimation of Γ, so we tried several values to find the approximate value. A set of curves describing eq 1 for different values of homogeneous broadening Γ, taken to be similar to the full low-energy absorption peak line width, is shown in Figure 4. Several important inferences can be drawn from Figure 4 without the exact knowledge of Γ. First, it is clearly seen that within the frame of this model it is impossible to have an anisotropy decay time of 40 fs and reside in the Förster regime (small interaction) for any homogeneous broadening smaller than the full line width. This supports the idea that coherence must be taken into account. Extrapolation of the Γ = 2000−3000 cm^{-1} curves to estimate the interaction strength results in a magnitude of J close to 1400 cm^{-1} (Figure 4). This estimated intracycle electronic coupling strength is much higher than that for interchromophore coupling for the natural photosynthetic ring LH2 (~300 cm^{-1}),[35,57] which is not surprising taking into account the π-conjugation in the 12mer.

Ultrafast Time-Resolved Fluorescence. An isotropic (magic angle) fluorescence decay profile for the 30mer at a detection wavelength of 570 nm is shown in Figure 5. The biexponential decay fit shows a long decay component near 361 ± 50 ps. This is

dx.doi.org/10.1021/ja108359w | J. Am. Chem. Soc. 2011, 133, 4819–4828

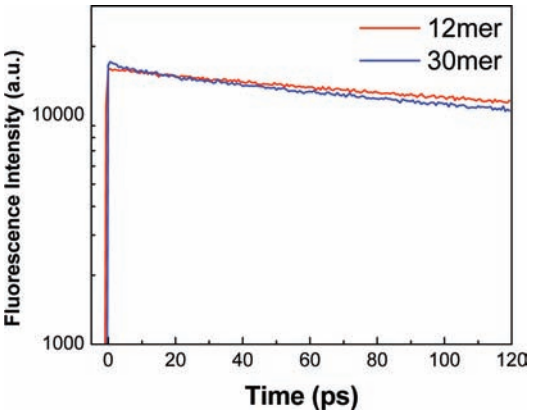

Figure 5. Fluorescence decay profiles for 12mer and 30mer. Excitation wavelength is 400 nm. Detection wavelengths are 570 nm.

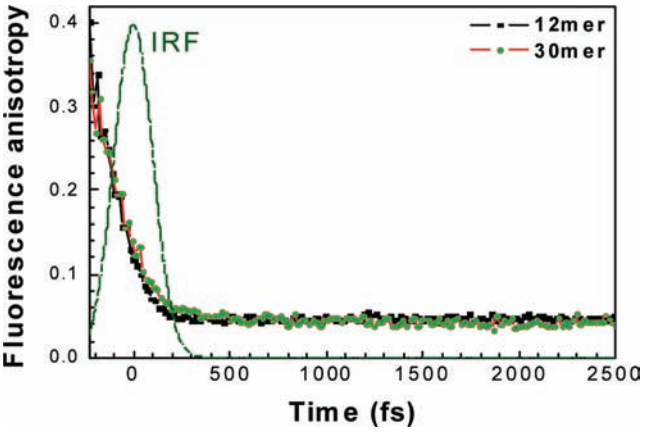

Figure 6. Time-resolved fluorescence anisotropy for 12mer and 30mer. Instrument response function (IRF) is also shown by dashed−dotted line.

very close to the fluorescence decay times obtained for linear oligo(thienylene-ethynylene)s (300−330 ps).[50] Similar to other oligo- and polythiophene systems, the fluorescence lifetime of the macrocycle is determined by the fluorescence quenching due to the intersystem crossing process.[11,26,50,58,59] Additionally, from our fluorescence decay measurements, the short decay component was found to be dependent on detection wavelength. For example, at 550 nm, we saw an initial decay component of ∼8 ps, while at 570 nm the initial component is closer to 14 ps (not shown). This behavior is typically associated with the dynamic Stokes shift. This can be caused by excitation energy migration along the chain, torsional relaxtion,[11,26,60−62] or solvation effects.[63] However, the transient absorption anisotropy measurement for the 12mer, as described above, indicates negligible energy migration along the thiophene ring chain on the picosecond time scale (Figure 3). Also, the hopping component for the 30mer has a time scale of ∼1 ps, which is substantially smaller than the short decay component of the fluorescence decay (Figure 3). It has also been shown that solvation effects are only a minor contributor to the dynamics of large conjugated oligomers and polymers.[52] For these reasons, we can conclude that the fast component in the isotropic decay (Figure 4) is most likely associated with a torsional relaxation in the excited state.[60−62] This process is caused by the difference in the torsional potential energy profile between the ground and excited states.[62,64]

Time-resolved fluorescence anisotropy measurements for the four macrocycles were also preformed. Figure 6 shows a comparison of the 12mer and 30mer anisotropy decay. Fast initial anisotropy decay within the instrument response profile, followed by a residual, relatively long-lived anisotropy, can be seen. This is qualitatively similar to what is observed in the transient absorption signal (Figure 3). However, in the case of fluorescence, most of the initial anisotropy at time zero that is seen in the transient absorption profile is lost in the higher lying states before relaxation to the fluorescent state. The residual anisotropy value, prior to rotational diffusion, for fluorescence (∼0.05) is lower than that for absorption (∼0.1). This difference likely arises due to the final arrangement of transition dipoles, which can be different for a relaxed fluorescence state as compared to a Franck−Condon absorption configuration. The transient absorption anisotropy measurement probes the excitation while it is delocalized across a large portion of the ring. In this delocalized configuration, the transition dipoles are arranged within the plane of the molecule, and the resulting long time anisotropy value is 0.1. In the time-resolved fluorescence anisotropy measurements, the lower value of 0.05 can be a signature of either an incline in the angle of the transition moment of the localized fluorescent state from the molecular plane[17,65] or a distortion of the molecule's shape in the relaxed fluorescent excited state from a planar configuration.

When discussing the fluorescence of these materials, it is worth noting that the fluorescence decay time in linear oligomers is very close to that for the rings,[50] while the fluorescence quantum yield for the rings was found to be almost 3 times smaller (∼10% in the rings, while ∼30% in the linear structures).[24,28,50] This suggests a smaller radiative decay rate for the rings as compared to their linear counterparts. In circular aggregates, the superradiance factor (the radiative rate enhancement factor with respect to that for the monomer) behaves differently as a function of size and disorder than in linear oligomers due to specific cyclic geometry.[37,66] The lowest transition is forbidden by symmetry considerations in ideal cyclic aggregates.[37,66] This specifically leads to the reduction of the radiative decay rate in circular aggregates as compared to linear oligomers.[37]

As was mentioned above, the fast component of the isotropic decay is likely due to a torsional relaxation in the excited state that results from a difference in the torsional potential energy profile between the ground and excited states. For linear oligo- and polythiophenes, a thiophene rotational potential energy profile in the excited state is steep, having its minimum at an inter-thiophene angle of 0°, while it is relatively shallow in the ground state with minima at ∼30° and ∼150°, corresponding to syn (*s*-cisoid) and anti (*s*-transoid) configurations, respectively.[60−62] This leads to a planarization of the structure after optical excitation, which produces the dynamic Stokes shift.[60] This situation looks more complex in oligo(thienylene-ethynylene)s. Calculations and X-ray analysis showed that linear oligo-(thienylene-ethynylene)s are near planar and mostly in anti configuration in the ground state.[50] In cyclic oligothiophene structures, geometrical and strain considerations predicted mostly syn configurations for smaller rings and anti configurations for larger (>14 thiophenes) rings.[49] In oligo(thienylene-ethynylene) cyclic systems containing 10 thiophenes, the X-ray analysis showed that all sulfur atoms in the thiophene rings were directed toward the cycle's center (syn configuration).[28] For the 12mer, similar analysis revealed that two thiophene rings from the total 12 are in *s*-transoid form with the sulfur atom directed

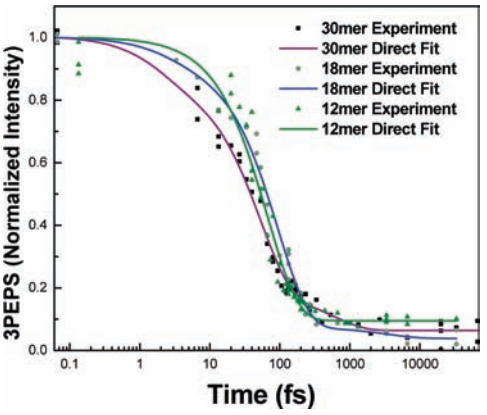

Figure 7. Comparison of direct fits of 3PEPS decay for thiophene macrocycles.

outside the macrocycle.[24] Both experiments indicated a near planar (not twisted) thiophene ring arrangement in the ground state for the macrocycles. For the larger rings, the molecular structure has not been yet determined by X-ray analysis. All of the larger rings have HOMO−LUMO gaps (from the absorption maxima, Figure 2) quite similar to each other but smaller than that of the 12mer. This can indicate a different conformational (torsional) arrangement for the larger macrocycles (18mer, 24mer, and 30mer) as compared to the 12mer. Calculations have shown that the difference in the HOMO−LUMO energy gap between syn and anti arrangements for large macrocyclic cyclo[*n*]thiophenes ($n > 20$) is relatively small; however, in terms of total strain energy, the anti configuration is more stable.[49] For large macrocyclic cyclo[*n*]thiophenes, the planarization of the thiophene rings system in the LUMO state for the anti configuration, similar to that for linear oligothiophenes, has also been predicted.[49] Rotational barriers and energy difference between the *s*-transoid and *s*-cisoid conformers are relatively small[12,49] and a mixed *s*-transoid and *s*-cisoid structure can be suggested for larger macrocycles. Moreover, taking into account low rotation barriers, torsional relaxation between conformers can occur after the excitation and contribute to the dynamic Stokes shift.

Three-Pulse Photon Echo Peak Shift. A comparison of the normalized three-pulse photon echo peak shift (3PEPS) decays of the macrocycles of different sizes is shown in Figure 7. Results of the direct fit of these raw data sets, along with a sum of exponentials, were used as initial parameters in determining our model for the transition frequency correlation function $M(t)$ given below. From Figure 7, it can be seen that the 3PEPS profile decays demonstrate clear ring-size dependence.

In order to better understand the dynamics of optical excitations, in regard to the nature of interaction between individual chromophores and between chromophores and solvent, we have preformed 3PEPS experiments[39,40] using an excitation wavelength of 415 nm. It should be noted that using an excitation wavelength that lies on the blue side of the molecules maximum absorption will have an excess of excitation energy that can have effects on the peak shift.[67] Additional vibrational modes can be excited and increase the number of dynamic processes occurring, resulting in smaller initial peak shift and reduced time constants.[68] However, because the absorption maxima of our systems are all quite similar (excluding the 12mer), by exciting

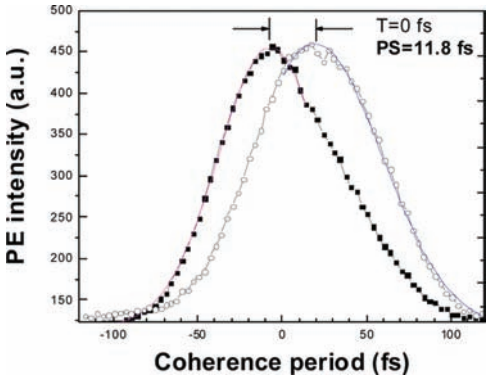

Figure 8. Three-pulse photon echo signal for 30mer at zero population period $T = 0$.

each system at 415 nm, we are providing approximately the same amount of excess energy for each system. Because our study is comparative in nature, we believe this excess of energy is not detrimental to our experiment or the context of our observed trends.

The 3PEPS method is capable of providing time scales and coupling strengths of dephasing processes that are coupled to electronic transitions by providing a line shape function and separating the static contribution to the line broadening.[39,40] A representative integrated three-pulse photon echo signal for the 30mer at $T = 0$ fs is shown in Figure 8. The 3PEPSs as functions of population period T for the 12mer and the 30mer are shown in parts a and b of Figure 9, respectively (data points). Numerical modeling of the echo peak shift was also performed using a direct fit of the raw peak shift data as initial parameters. We started from a model for the transition frequency correlation function $M(t)$ for a two-level chromophore coupled to the environment and to its own fluctuating nuclei:

$$M(t) = \frac{\langle \delta\omega(0)\delta\omega(t)\rangle}{\langle \delta\omega^2\rangle}$$

where $\delta\omega(t)$ is the fluctuating part of the electronic transition frequency for each chromophore relative to its central frequency $\langle\omega\rangle$. Beyond the pulse overlap time interval, an initial guess of the energy gap correlation function $M(t)$ can be obtained that closely follows the experimental 3PEPS profile.[38−40] The quantity $M(t)$ is important because it can be used for the description of the memory of the electronic transition frequency and system dynamics when the characteristic frequencies of the transition frequency fluctuations are small compared to kT.[43] This high-temperature approach can be applied to describe the coupling of the electronic transition to many intermolecular (solvation) modes at room temperature. The main spectroscopic signals can be most conveniently derived from the complex line shape function $g(t)$:[43]

$$g(t) = P(t) + iQ(t)$$
$$= \langle \Delta\omega^2\rangle \int_0^t dt_1 \int_0^{t_1} dt_2\, M(t_2) + i\lambda \int_0^t dt_1\, M(t_1) \qquad (2)$$

In eq 2, $P(t)$ and $Q(t)$ are the real and imaginary parts of $g(t)$, $\langle\Delta\omega^2\rangle$ is the coupling strength (fluctuation amplitude), and λ is the reorganization energy. The absorption spectrum of the system can be calculated by taking the real part of the Fourier transform of $\exp[-g(t)]$, while the third-order photon echo

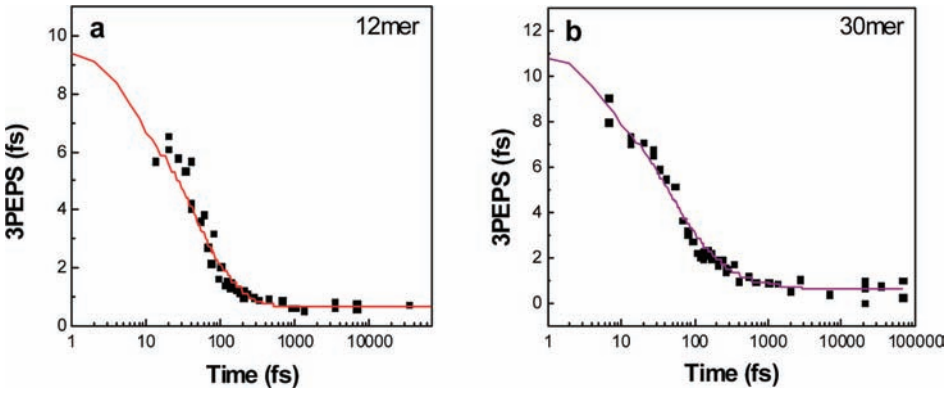

Figure 9. Three-pulse photon echo peak shift profiles for 12mer and 30mer. Numerical modeling results are also shown (solid lines).

signal in the impulsive limit can be expressed by[38−40,45,46]

$$S_{PE}(\tau, T) \propto \int_0^\infty dt \exp[-\sigma_{in}{}^2(t-\tau)^2] \exp\{-2[P(\tau) - P(T) + P(t) + P(\tau+T) + P(T+t) - P(\tau+T+t)]\} \cos^2[Q(T) + Q(t) - Q(T+t)] \quad (3)$$

where σ_{in} represents the width of the static inhomogeneous distribution.

Using the model described above, the peak shift values (position of the maximum, τ_p) were calculated from the photon echo signal $S_{PE}(\tau,T)$ for the 12mer and 30mer as a function of population period T and are shown in Figure 9 (solid lines). Most of the modeling was performed using the impulsive limit, but the effect of the finite pulse width was considered and estimated by convoluting the pulse electric field envelope (which was taken to be of Gaussian shape with σ = 35 fs) with the proper time-ordered[38−40] response functions (for positive τ, the rephasing response functions contribute, while for negative τ, the non-rephasing response functions contribute) at several population periods (T-points). These response functions were then used to determine the third-order polarization, which was used to calculate the time-integrated photon echo signal with a finite pulse width.[39] These convoluted values were then compared to the 3PEPS values obtained in the impulsive limit and the ratio $3PEPS_{conv}/3PEPS_{impuls}$ was found. This ratio was determined to be weakly dependent on the population period T, and we corrected the impulsive limit results by this factor.[38,45,46,68] Using too many parameters in the model correlation function can result in different contributions canceling one another out. To minimize such issues, we have attempted to limit the various contributions to $M(t)$ to three exponentials and one constant (static disorder):

$$M(t) = \frac{\left[\sum_{i=1}^{3} \langle \Delta\omega_{ei}{}^2 \rangle \exp\left(-\frac{t}{\tau_{ei}}\right) + \sigma_{inh}{}^2\right]}{\left[\sum_{i=1}^{3} \langle \Delta\omega_{ei}{}^2 \rangle + \sigma_{inh}{}^2\right]} \quad (4)$$

In some cases, a Brownian oscillator was added to the model. In effect, the Brownian oscillator contribution qualitatively represents a sum of several intramolecular vibrational modes that are not exactly known for these macrocycles.[69] From Figure 9, it is clear that there is good agreement between the experimental data points and the modeled fit. The time constants and coupling strengths of the model $M(t)$ are shown in Table 1.

Table 1

macrocycle	$\Delta\omega_1$, cm^{-1}	τ_1, fs	$\Delta\omega_2$, cm^{-1}	τ_2, fs	$\Delta\omega_3$, cm^{-1}	τ_3, fs	σ_{inh}, cm^{-1}
12mer	503	4	476	130	0	−	291
30mer	450	4.8	370	140	212	800	238

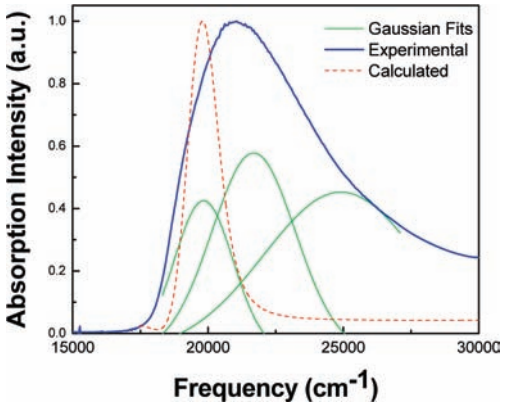

Figure 10. Comparison of experimental and calculated absorption spectrum for the 30mer.

Once a set of parameters was obtained that reproduced a satisfactory peak shift, the absorption spectrum was calculated for the 30mer and compared with the experimental spectrum. It can be seen in Figure 10 that the calculated absorption spectrum is noticeably narrower than the full experimental absorption spectrum. In order to better understand the structure of the experimental absorption spectrum, we performed a simple decomposition of the spectra using three Gaussian components. By comparing the absorption spectrum calculated from the correlation function obtained from the 3PEPS experiments, we see some similarity in the calculated spectrum and the first Gaussian component, though a vibronic progression is not clearly seen.

Previous work[39,40] has shown that residual 3PEPS at very large population periods results from static inhomogeneous broadening. From Figure 9, it can be seen that the residual 3PEPS is very small for all investigated macrocycles. This indicates minor inhomogeneous broadening (conformational diversity) for all studied systems.[38,39] It is also known that the initial peak shift reflects the inverse effective electronic transition−bath

dx.doi.org/10.1021/ja108359w |J. Am. Chem. Soc. 2011, 133, 4819–4828

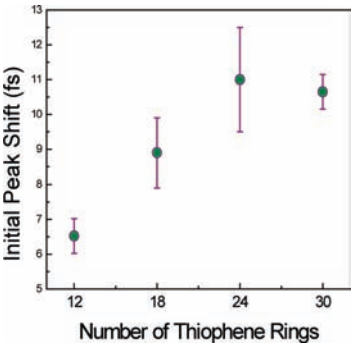

Figure 11. Three-pulse photon echo initial peak shift as a function of the ring size.

interaction.[38−40] Our results clearly show an increase in initial peak shift as ring size is increased (Figure 11). This rise in peak shift indicates a decrease of the effective electron−bath coupling for larger rings. This is a counterintuitive trend, as the complexity of the system is rising with increased ring size, leading one to expect increased disorder and increased coupling pathways to the bath. We propose that this weaker coupling is the result of exchange narrowing effects, which are caused by the eigenstate averaging over the fluctuations and local inhomogeneities of the sites by delocalized excitation.[36,41−43] Exchange narrowing occurs and the fluctuations of the system average out such that interaction with the bath decreases with an increase in ring size.[36,45,46] Also, the 3PEPS decays very quickly as a function of population period. The decay profile shows only minor contribution from the subpicosecond and picosecond components. From this, it is clear that most of the dephasing in these large macrocycles can be associated with intramolecular processes rather than solvation, similar to what was reported for polymers,[52] dendrimers,[45] and J-aggregates.[69]

After considering what has been learned from the transient absorption and fluorescence upconversion experiments, we can use our 3PEPS experimental results and numerical modeling to gain a detailed perspective of the excited-state dynamics occurring in the thiophene macrocycles. Three distinct time constants were seen in the numerical modeling of the 3PEPS signal. Though these time constants do not align exactly with those provided by our transient absorption and fluorescence upconversion experiments, we believe the first two exponential time components of our numerical model may be revealing some combination of high-frequency vibrational modes and self-trapping of excitation along the macrocycle. Previous results have shown self-trapping to occur in <45 fs.[52,70,71] In our numerical model, we cannot clearly distinguish between the two processes, but it is likely that the faster time constant is representative of a self-trapping process. The 3PEPS numerical modeling also indicated the presence of a picosecond component in the correlation function for the larger macrocycles (18mer, 24mer, and 30mer), which is absent for the smaller 12mer macrocycle. This correlates well with the ultrafast fluorescence anisotropy data. These findings support the suggestion of an initially delocalized excitation over a major fraction of the ring, followed by incoherent hopping taking place on a picosecond time scale.

Comparison to Natural Light-Harvesting Systems. When considering their potential for application in the future, it is beneficial to compare these systems with natural light-harvesting antenna, like LH2 of purple photosynthetic bacteria. In comparison to the natural system, our synthetic system has dramatically increased interaction strength between chromophores. As a result, our synthetic system demonstrates enhancement of several optical properties over the natural system. The excitation transfer time of our synthetic system is 40 fs, as compared to 700 fs[72] in the natural system. The TPA cross section of our synthetic system is 2 orders of magnitude higher than that of the natural system.[24,73] The excitation delocalization length for our synthetic system is 18 units, which is dramatically larger than that of the natural system.[37] Though these materials are still quite far from mimicking the high efficiency of a natural system, their optical properties, as seen in Table 2, clearly demonstrate they are a material of interest for future work.

Table 2

	light-harvesting pigments	
	LH2 of purple photosynthetic bacteria	synthetic 30mer
transfer time[a]	700 fs[72]	40 fs
initial peak shift	24 fs[72]	12 fs
interaction strength	320 cm^{-1} (intra), 255 cm^{-1} (inter)[35]	1500 cm^{-1}
TPA cross section	1116 GM (calculated)[73]	107 800 GM[24]
line width	~450 cm^{-1}[72]	~2000 cm^{-1}
excited state lifetime	1 ns[74]	~300 ps
delocalization length	5−13 units[37]	18 units

[a] From depolarization measurements.

CONCLUSION

In this work, we have presented a detailed study of the excited-state structure and dynamics in a series of large oligo(thienylene-ethynylene) macrocycles. We have brought together a variety of recent synthetic and spectroscopic techniques, combined with theoretical modeling, to closely describe the delocalized excitations in a series of macrocyclic thiophene systems. The three-pulse photon echo peak shift experiments showed a clear dependence of the initial peak shift on ring size. The rise of the peak shift with the ring size suggests the tendency to decrease effective electron−bath coupling for larger delocalization lengths in large macrocycles. From depolarization experiments, we see a planar arrangement of the transition dipoles (in the absorption configuration) even in large rings. We also show from photon echo experiments that there is low inhomogeneous broadening for all systems. Combined, these results indicate relatively ordered structures. Collectively, our experimental results indicate that a delocalized state can be seen upon excitation of the cyclic thiophene rings, which we estimate has a length of about 18 (theienylene-ethynylene) units for the thiophene system. This conclusion is in accord with a strong cooperative enhancement of two-photon absorption cross-section in the 18mer reported previously.[24] Also, by comparing the optical properties of our synthetic pigment to a natural light-harvesting system, we have demonstrated the utility of these materials for future applications. It is our hope that the results offered here will lend themselves to the future development of the next generation of solar conversion devices.

ASSOCIATED CONTENT

Supporting Information. Details of fwhm comparison for all rings, as well as the anisotropy best fit procedure available.

This material is available free of charge via the Internet at http://pubs.acs.org/.

AUTHOR INFORMATION

Corresponding Author
tgoodson@umich.edu

ACKNOWLEDGMENT

T.G. III acknowledges NSF (polymer) and Air Force AFOSR (Organic Materials Chemistry) for support.

REFERENCES

(1) Collini, E.; Wong, C. Y.; Wilk, K. E.; Curmi, P. M. G.; Brumer, P.; Scholes, G. D. *Nature* **2010**, *463*, 644.
(2) Engel, G. S.; Calhoun, T. R.; Read, E. L.; Ahn, T. K.; Mancal, T.; Cheng, Y. C.; Blankenship, R. E.; Fleming, G. R. *Nature* **2007**, *446*, 782.
(3) van Grondelle, R.; Novoderezhkin, V. I. *Nature* **2010**, *463*, 614.
(4) Lee, H.; Cheng, Y. C.; Fleming, G. R. *Science* **2007**, *316*, 1462.
(5) Cheng, Y. C.; Silbey, R. J. *Phys. Rev. Lett.* **2006**, *96*, 028103.
(6) Ishizaki, A.; Fleming, G. R. *Proc. Natl. Acad. Sci. U.S.A.* **2009**, *106*, 17255.
(7) Scholes, G. D. *J. Phys. Chem. Lett.* **2010**, *1*, 2.
(8) Lightowler, S.; Hird, M. *Chem. Mater.* **2005**, *17*, 5538.
(9) Mishra, A.; Ma, C. Q.; Bauerle, P. *Chem. Rev.* **2009**, *109*, 1141.
(10) Ma, W. L.; Yang, C. Y.; Gong, X.; Lee, K.; Heeger, A. J. *Adv. Funct. Mater.* **2005**, *15*, 1617.
(11) Ramakrishna, G.; Bhaskar, A.; Bauerle, P.; Goodson, T. *J. Phys. Chem. A* **2008**, *112*, 2018.
(12) Mena-Osteritz, E. *Adv. Mater.* **2002**, *14*, 609.
(13) Cho, S.; Seo, J. H.; Park, S. H.; Beaupre, S.; Leclerc, M.; Heeger, A. J. *Adv. Mater.* **2010**, *22*, 1253.
(14) BarHaim, A.; Klafter, J.; Kopelman, R. *J. Am. Chem. Soc.* **1997**, *119*, 6197.
(15) Devadoss, C.; Bharathi, P.; Moore, J. S. *J. Am. Chem. Soc.* **1996**, *118*, 9635.
(16) Hagedorn, K. V.; Varnavski, O.; Hartwig, J.; Goodson, T. *J. Phys. Chem. C* **2008**, *112*, 2235.
(17) Varnavski, O. P.; Ostrowski, J. C.; Sukhomlinova, L.; Twieg, R. J.; Bazan, G. C.; Goodson, T. *J. Am. Chem. Soc.* **2002**, *124*, 1736.
(18) Poliakov, E. Y.; Chernyak, V.; Tretiak, S.; Mukamel, S. *J. Chem. Phys.* **1999**, *110*, 8161.
(19) Minami, T.; Tretiak, S.; Chernyak, V.; Mukamel, S. *J. Lumin.* **2000**, *87*−*89*, 115.
(20) Kirkwood, J. C.; Scheurer, C.; Chernyak, V.; Mukamel, S. *J. Chem. Phys.* **2001**, *114*, 2419.
(21) Bosman, A. W.; Janssen, H. M.; Meijer, E. W. *Chem. Rev.* **1999**, *99*, 1665.
(22) Sundström, V.; Pullerits, T.; van Grondelle, R. *J. Phys. Chem. B* **1999**, *103*, 2327.
(23) Bradforth, S. E.; Jimenez, R.; Vanmourik, F.; van Grondelle, R.; Fleming, G. R. *J. Phys. Chem.* **1995**, *99*, 16179.
(24) Williams-Harry, M.; Bhaskar, A.; Ramakrishna, G.; Goodson, T.; Imamura, M.; Mawatari, A.; Nakao, K.; Enozawa, H.; Nishinaga, T.; Iyoda, M. *J. Am. Chem. Soc.* **2008**, *130*, 3252.
(25) Varnavski, O.; Bauerle, P.; Goodson, T. *Opt. Lett.* **2007**, *32*, 3083.
(26) Bhaskar, A.; Ramakrishna, G.; Hagedorn, K.; Varnavski, O.; Mena-Osteritz, E.; Bauerle, P.; Goodson, T. *J. Phys. Chem. B* **2007**, *111*, 946.
(27) Raymond, J. E.; Bhaskar, A.; Goodson, T.; Makiuchi, N.; Ogawa, K.; Kobuke, Y. *J. Am. Chem. Soc.* **2008**, *130*, 17212.
(28) Nakao, K.; Nishimura, M.; Tamachi, T.; Kuwatani, Y.; Miyasaka, H.; Nishinaga, T.; Iyoda, M. *J. Am. Chem. Soc.* **2006**, *128*, 16740.
(29) Iyoda, M. *Heteroat. Chem.* **2007**, *18*, 460.
(30) Zhang, F.; Gotz, G.; Winkler, H. D. F.; Schalley, C. A.; Bauerle, P. *Angew. Chem., Int. Ed.* **2009**, *48*, 6632.
(31) Kromer, J.; Rios-Carreras, I.; Fuhrmann, G.; Musch, C.; Wunderlin, M.; Debaerdemaeker, T.; Mena-Osteritz, E.; Bauerle, P. *Angew. Chem., Int. Ed.* **2000**, *39*, 3481.
(32) Wynands, D.; Mannig, B.; Riede, M.; Leo, K.; Brier, E.; Reinold, E.; Bauerle, P. *J. Appl. Phys.* **2009**, *106*, 054509.
(33) Van Patten, P. G.; Shreve, A. P.; Lindsey, J. S.; Donohoe, R. J. *J. Phys. Chem. B* **1998**, *102*, 4209.
(34) Leegwater, J. A. *J. Phys. Chem.* **1996**, *100*, 14403.
(35) Scholes, G. D.; Fleming, G. R. *J. Phys. Chem. B* **2000**, *104*, 1854.
(36) Beljonne, D.; Curutchet, C.; Scholes, G. D.; Silbey, R. J. *J. Phys. Chem. B* **2009**, *113*, 6583.
(37) Dahlbom, M.; Pullerits, T.; Mukamel, S.; Sandström, V. *J. Phys. Chem. B* **2001**, *105*, 5515.
(38) Cho, M. H.; Yu, J. Y.; Joo, T. H.; Nagasawa, Y.; Passino, S. A.; Fleming, G. R. *J. Phys. Chem.* **1996**, *100*, 11944.
(39) Joo, T. H.; Jia, Y. W.; Yu, J. Y.; Lang, M. J.; Fleming, G. R. *J. Chem. Phys.* **1996**, *104*, 6089.
(40) deBoeij, W. P.; Pshenichnikov, M. S.; Wiersma, D. A. *J. Phys. Chem.* **1996**, *100*, 11806.
(41) Kubo, R. *Adv. Chem. Phys.* **1969**, *15*, 101.
(42) Knapp, E. W. *Chem. Phys.* **1984**, *85*, 73.
(43) Ohta, K.; Yang, M.; Fleming, G. R. *J. Chem. Phys.* **2001**, *115*, 7609.
(44) Demas, J. N.; Crosby, G. A. *J. Phys. Chem.* **1971**, *75*, 991.
(45) Varnavski, O.; Yan, X. Z.; Mongin, O.; Blanchard-Desce, M.; Goodson, T. *J. Phys. Chem. C* **2007**, *111*, 149.
(46) Varnavski, O.; Goodson, T.; Sukhomlinova, L.; Twieg, R. *J. Phys. Chem. B* **2004**, *108*, 10484.
(47) Varnavski, O.; Goodson, T.; Bauerle, P. *Linear and Nonlinear Optics of Organic Materials VII* **2007**, *6653*, 65317.
(48) Shah, J. *IEEE J. Quant. Elec.* **1988**, *24*, 276.
(49) Zade, S. S.; Bendikov, M. *J. Org. Chem.* **2006**, *71*, 2972.
(50) Fujitsuka, M.; Makinoshima, T.; Ito, O.; Obara, Y.; Aso, Y.; Otsubo, T. *J. Phys. Chem. B* **2003**, *107*, 739.
(51) Li, J.; Liao, L.; Pang, Y. *Tetrahedron Lett.* **2002**, *43*, 391.
(52) Yang, X. J.; Dykstra, T. E.; Scholes, G. D. *Phys. Rev. B* **2005**, *71*, 045203.
(53) Heimel, G.; Daghofer, M.; Gierschner, J.; List, E. J. W.; Grimsdale, A. C.; Mullen, K.; Beljonne, D.; Bredas, J. L.; Zojer, E. *J. Chem. Phys.* **2005**, *122*, 054501.
(54) Hall, R. D.; Valeur, B.; Weber, G. *Chem. Phys. Lett.* **1985**, *116*, 202.
(55) Chang, R.; Hsu, J. H.; Fann, W. S.; Liang, K. K.; Chiang, C. H.; Hayashi, M.; Yu, J.; Lin, S. H.; Chang, E. C.; Chuang, K. R.; Chen, S. A. *Chem. Phys. Lett.* **2000**, *317*, 142.
(56) Beenken, W. J. D.; Pullerits, T. *J. Phys. Chem. B* **2004**, *108*, 6164.
(57) Tretiak, S.; Middleton, C.; Chernyak, V.; Mukamel, S. *J. Phys. Chem. B* **2000**, *104*, 4519.
(58) Becker, R. S.; deMelo, J. S.; Macanita, A. L.; Elisei, F. *J. Phys. Chem.* **1996**, *100*, 18683.
(59) Magnani, L.; Rumbles, G.; Samuel, I. D. W.; Murray, K.; Moratti, S. C.; Holmes, A. B.; Friend, R. H. *Synth. Met.* **1997**, *84*, 899.
(60) Westenhoff, S.; Beenken, W. J. D.; Friend, R. H.; Greenham, N. C.; Yartsev, A.; Sundström, V. *Phys. Rev. Lett.* **2006**, *97*, 166804.
(61) Lanzani, G.; Nisoli, M.; DeSilvestri, S.; Tubino, R. *Chem. Phys. Lett.* **1996**, *251*, 339.
(62) Grozema, F. C.; van Duijnen, P. T.; Berlin, Y. A.; Ratner, M. A.; Siebbeles, L. D. A. *J. Phys. Chem. B* **2002**, *106*, 7791.
(63) Horng, M. L.; Gardecki, J. A.; Papazyan, A.; Maroncelli, M. *J. Phys. Chem.* **1995**, *99*, 17311.
(64) Beenken, W. J. D.; Lischka, H. *J. Chem. Phys.* **2005**, *123*, 9.
(65) Demidov, A. A.; Andrews, D. L. *Photochem. Photobiol.* **1996**, *63*, 39.
(66) Bednarz, M.; Reineker, P.; Mena-Osteritz, E.; Bauerle, P. *J. Lumin.* **2004**, *110*, 225.
(67) Larsen, D. S.; Ohta, K.; Xu, Q.-H.; Cyrier, M.; Fleming, G. R. *J. Chem. Phys.* **2001**, *114*, 8008.

(68) Nagasawa, Y.; Passino, S. A.; Joo, T.; Fleming, G. R. *J. Chem. Phys.* **1997**, *106*, 4840.
(69) Mukamel, S. *Principles of Nonlinear Optical Spectroscopy*; Oxford University Press, Inc.: New York, 1995.
(70) Grage, M. M. L.; Zaushitsyn, Y.; Yartsev, A.; Chachisvilis, M.; Sundström, V.; Pullerits, T. *Phys. Rev. B* **2003**, *67*, 205207.
(71) Sperling, J.; Nemeth, A.; Baum, P.; Sanda, F.; Riedle, E.; Kauffmann, H. F.; Mukamel, S.; Milota, F. *Chem. Phys.* **2008**, *349*, 244.
(72) Jimenez, R.; vanMourik, F.; Yu, J. Y.; Fleming, G. R. *J. Phys. Chem. B* **1997**, *101*, 7350.
(73) Abe, S. *Chem. Phys.* **2001**, *264*, 355.
(74) Freiberg, A.; Jackson, J. A.; Lin, S.; Woodbury, N. W. *J. Phys. Chem. A* **1998**, *102*, 4372.